A laboratory study of acoustic behaviors of bubbles caused by oil leakages

Zhiqu Lu[a], National Center for Physical Acoustics, The University of Mississippi, University, MS, 38677 zhiqulu@olemiss.edu

Xudong Fan, The Department of Physics, The University of Mississippi, University, MS, 38677 xfan1@go.olemiss.edu

Likun Zhang, The Department of Physics, The University of Mississippi, University, MS, 38677 zhang@olemiss.edu

Running title: acoustic behaviors of oil leakage bubbles

[a]Author to whom correspondence should be addressed. ORCID: 0000-0002-5747-0455

Abstract: The growth of oil production increases the risk of oil leakage. Along with the spilling processes, natural gases create underwater sounds due to bubble oscillations, which can be recorded and utilized to detect, locate, and assess the leakage event for a real-time monitoring system. For this paper, a laboratory study was conducted to simulate oil leakages under controlled conditions in order to gain a fundamental understanding of the bubble induced sounds. Empirical relationships were found among the resonant frequency, total energy, flow rate, and needle diameter. A simple model for bubble-induced sounds in terms of the total energy was obtained.

Keywords: underwater sound, bubbles, oil leakage, water tank, hydrophone

1. Introduction

The rapid growth of oil and gas production in the Gulf of Mexico increases the risk of oil spills at greater water depths and drilling wells. These hydrocarbon leakages can be caused by either natural events, such as seeping from fissures in the seabed and eroding sedimentary rocks (http://www.soscalifornia.org/natural-oil-seepage-facts/), or by anthropogenic accidents, such as leaking from broken wellheads and pipelines by mechanical failures - like the Macondo well blowout and Deepwater Horizon explosion in April 2010 [Deepwater Horizon Study Group, 2011]. In order to improve safety and reduce environmental damages of offshore oil and gas operations, the Bureau of Safety and Environmental Enforcement of the U.S. Department of the Interior recommended the use of real-time monitoring [Transportation Research Board Special Report 322, 2016]. An early warning system for detecting, locating, and characterizing hydrocarbon leakages is essential for preventing the next oil spill as well as for seafloor hydrocarbon seepage detection.

In an oil leakage event, the spilled crude oil is a mixture of natural gases and oils with considerable amounts of gases (a reported gas-to-oil ratio of 1,600 ft^3/bbl and 82.5% of methane for the total natural gas compositions, [Reddy *et al*., 2012]). At the initial stage, oil droplets and gas bubbles discharge from a leaking point at high speeds. The gas bubbles experience dramatic shape deformations due to sudden changes in hydrostatic pressure and oil jet velocity, which trigger oscillations of gas bubbles and initiate the generation of bubble sounds [Leighton, 1994]. These oil spill-induced underwater acoustic emissions can be recorded by hydrophones in the water column at far distances due to low attenuation in seawater [Urick, 1983; Lurton, 2002]. They can be analyzed and characterized to provide information about the locations and properties of the leakages.

In 2017, an integrated research project (http://aduolp.olemiss.edu/) was funded to develop a hydrophone network-based real-time passive monitoring system for detecting, locating, and characterizing hydrocarbon leakage. One of the objectives of the project is to gain a fundamental understanding of the acoustic behaviors of bubbles due to oil leakage. To achieve this goal, a laboratory study was conducted and the results was reported in this paper. The study included the tasks of (1) simulating oil leakages under controlled conditions (such as gas pressures, flow rates, leak opening sizes, and types of leakages), (2) recording the oil leakage-induced sounds, and (3) establishing the correlation between frequency spectra and oil leakage properties, such as oil leakage flow rate and jet velocity, bubble radii and distributions, and crack sizes. Another objective of the project is leakage source localization, and its results will be reported elsewhere.

2. Experimental Setup

The experimental setup consists of a bubble generation system, a water tank, a hydrophone network, a data acquisition system, and an underwater camera.

In this study, two types of gas leakages were investigated: (1) a few bubble case to simulate oil seepage from fissures in the ocean seabed, and (2) a constant flow case to simulate gas leakage from broken wellheads or pipelines. A schematic diagram of the bubble generation system is shown in Fig. 1. For a few bubble case, a syringe pump (WPI, SP260P) was used as a small volume gas reservoir. The pump was flow rate controllable and programmed by a computer via RS232-2 interface and the gas under test was pushed with a syringe into the transport pipeline at very low flow rates in order to generate a single bubble or a few bubbles. For the constant flow bubble case, a compressed gas (either nitrogen or methane gas) cylinder

served as a large volume gas reservoir to introduce continuous and constant flow rates of gas into the pipeline. A pressure regulator/gauge adjusted manually the output pressure of the gas. A 3-way valve was employed to switch the connections among the syringe pump, gas cylinder, and pipelines. The pipelines were Plexiglas tubes. Two solenoid valves (Asco Red-Hat 8262H202 for Solenoid valve-1, Parker Hannifin 009-0272-900 for Solenoid valve-2) remotely opened and closed the pipeline. In between the two solenoid valves, a digital flowmeter (Aalborg, XFM17) was installed for flow rate measurement via a RS232-1 interface for the constant flow bubble case. Note that the flow rate for a few bubble case was controlled by the syringe pump with a pre-determined value. The gas under test was injected into the water column through a syringe needle. A check valve was used to prevent water from entering back into the needle. The syringe needle was replaceable with a variety of needle apertures. PVC pipes (6" in diameter) were used to construct a bubble generation enclosure to contain the bubble generation system and allow it to be submerged in the water tank. Several lead bricks were placed inside the enclosure to counteract the buoyancy force. The dimensions of the water tank were 2.13 m×2.13 m×1.83 m (7'×7'×6'). The tank was filled with tap water to a water level of 1.68 m. Two gases were employed for the tests: nitrogen and methane.

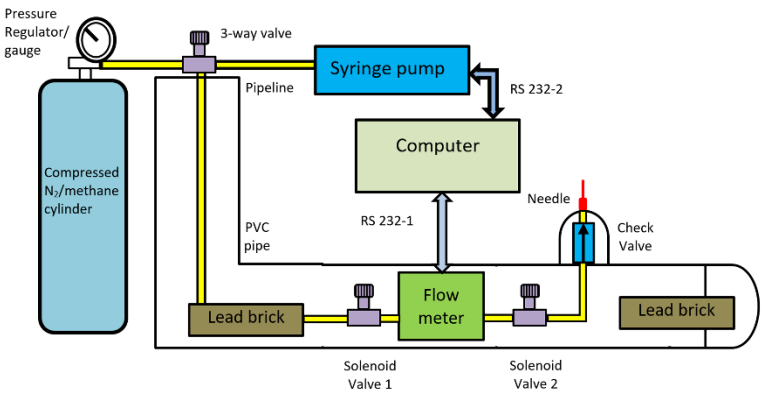

Fig. 1. (Color online) The schematic diagram of the bubble generation system.

Seven hydrophones (Aquarian, H1a) were randomly distributed around the needle in the water tank to form a hydrophone network for recording bubble sounds and for leakage source localization. They were amplified by hydrophone amplifiers (Aquarian Scientific, PA4-DC) and the signals were received at the input channels of two oscilloscopes (Agilent, infinium). The signal from one of the hydrophones was used as a trigger to synchronize the data acquisition. The signals were acquired and transferred to the computer *via* IEEE 488 interface. The whole measurement system was automated with a program written in LabView.

A digital underwater camera (Olympus, TG-5) recorded movies that captured the processes of bubble movements at 240 frame/s. Fig. 2(a) shows an example for a few bubbles case where two bubbles occur and Fig. 2(b) presents a typical photo of the constant flow bubble case where cloudy bubbles with different sizes appear. The corresponding sounds in both time and frequency domains are displayed in Figs. 2(c)-2(d).

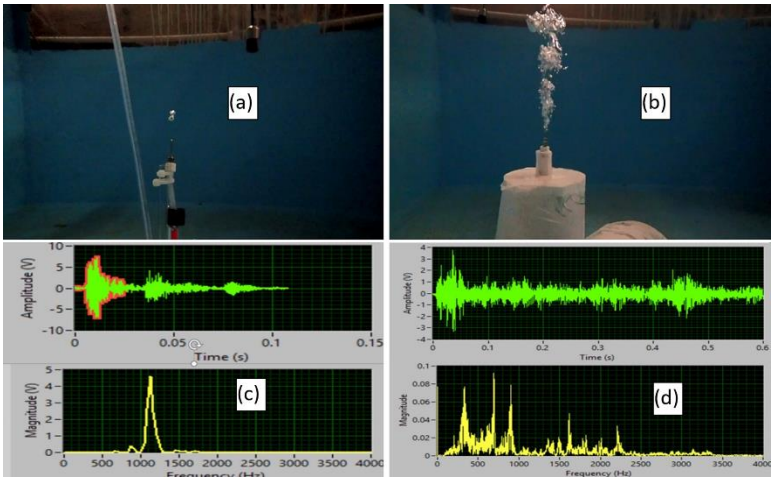

Fig. 2 (Color online) (a) the photo of a few bubble case, (b) the photo of the constant flow bubble case; (c) acoustic signals in time and frequency domains for a few bubble case, and (d) acoustic signals in time and frequency domains for the constant flow bubble case. In Fig. 2(c), the first predominant time trace was selected by a time window for determining the resonant frequency.

3. Results

3.1 A few bubble case

Two motivations served for this case study. One was to simulate seafloor seepage and the other was to establish the correlation between the resonant frequency and crack size. For the former, the syringe pump was programmed to yield very low flow rates ranging from 5μL/min to 200μL/min, attempting to generate a single bubble in a quasi-static manner. However, it was found that even at the lowest flow rate of 5μL/min, it was very difficult to generate a single bubble. In most cases, a few (two or three) bubbles emerged from the needle almost concurrently, as seen in Fig. 2(a). For the latter motivation, a number of syringe needles with standard gauge numbers from G12 to G24 were employed. These needles have a blunt tip.

The resonant frequency of an individual bubble event was obtained by selecting the first predominant time-trace of the bubble sound using a time window and performing a fast Fourier transform FFT as shown in Fig. 2(c). Because each bubble event often yielded slightly different frequency responses, tens of bubble events were recorded and their resonant frequencies were compiled in a histogram (not shown), where the peak of the histogram was determined as the resonant frequency for a specific needle and flow rate. The obtained resonant frequencies of both nitrogen and methane *vs* needle diameter along with the different flow rates are displayed in Fig.

3(a), where μL/min in the legend denotes the flow rate. No significant difference between nitrogen and methane was found at present testing conditions. The solid line in Fig. 3(a) is a regression curve, expressed by: $f = AD^{-1/3}$, where f is the resonant frequency, D is the diameter of needles, A is a constant, which yielded a coefficient of correlation $|r|^2$ of 0.8 and an A value of 1551. This regressed curve presents a nonlinear decreasing trend in the resonant frequency as the needle diameter increases, in good agreement with the theoretical prediction $f \propto D^{-1/3}$ [Longuet-Higgins *et al*, 1991]. Moreover, this observation could be useful in estimating a crack opening size from the recorded frequency.

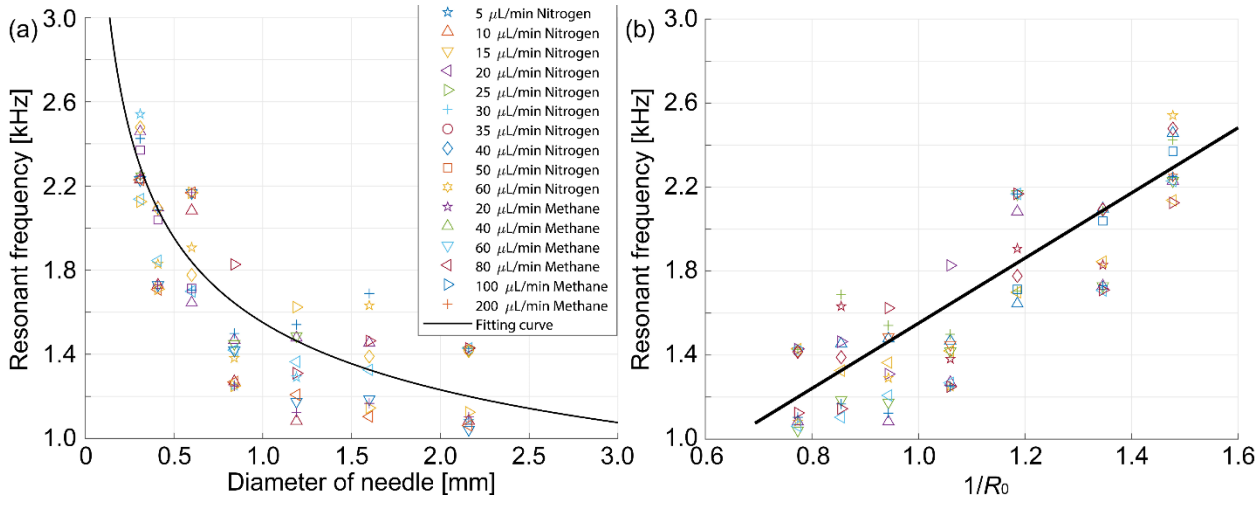

Fig.3 (Color online) (a) The resonant frequency *vs* the diameter of the needles, where μL/min in the legend denotes the flow rate and the solid line is the regression line, and (b) The resonant frequency *vs* $1/R_0$, where R_0 is the effective radius of a spherical bubble.

However, when one examines the data for a specific needle at different flow rates, the resonant frequencies are relatively scattered and no common trend can be found between the two parameters. As mentioned before, the bubbles were generated in a quasi-static manner at very low flow rates. Each bubble event occurred intermittently and was thus independent of the low

flow rates. Video recording (like Fig. 2(a)) revealed that the bubbles in different events featured slightly different shape deformations (non-spherical bubbles) and sizes even at the same flow rate. These inconsistencies among bubble events contribute to the scattering of the resonant frequency. For this reason a histogram method was used to determine the resonant frequency.

For a few bubbles case, the resonant frequency f is proportional to negative one third of the needle diameter D, in good agreement with the theoretical prediction by Longuet-Higgins *et al*. (1991). Furthermore, according their study, a single spherical bubble volume is proportional to the needle diameter. As such, the equation $f=AD^{-1/3}$ can be reduced into a formulae expressed by $f=A'/R_0$, where A' is an adjustable constant and R_0 is the effective bubble radius. This new equation is in the form of the well-known Minnaert (1933) resonant frequency for a pulsating spherical bubble. The resonant frequency *vs* $1/R_0$, is plotted in Fig. 3(b), where R_0 is the radius of a spherical bubble and the solid line is a linear regression with a coefficient of correlation of $|r|^2$ of 0.8.

3.2 The constant flow bubble case

For the constant flow bubble case, the gas under test was injected into the water at a constant flow rate. As seen in Fig. 2(b), the injected gas formed a cloud of bubbles with different bubble sizes which created a broadband signal with frequencies ranging from 300 Hz to 2500 Hz. This broadband signal features several distinctive frequency peaks that could be utilized to estimate the bubble size distributions [Leighton and Walton, 1987], which will be reported elsewhere. In this paper, we mainly focused our attention on the total energy and its relationship with flow rate and jet velocity. The total energy was defined as the summation of the squared frequency magnitude spectra over a certain frequency range, say from 300 Hz to 2500 Hz. The

duration of the time trace for the FFT was 0.3 s. The jet velocity was calculated by dividing the flow rate with the interior area of a needle.

Figure 4(a) shows the total energy *vs* flow rate and Fig. 4(b) displays the total energy *vs* jet velocity for both nitrogen and methane with different needle gauge numbers. Note that for nitrogen the syringe needle with G22 was tested whereas for methane the G21 syringe needle was used. As seen in Figs. 4(a)-4(b), the total energy increases with the flow rate and jet velocity. The trends of the total energy vs flow rate are spread widely among the different needles, whereas the total energy vs jet velocity curves seem closer to each other, implying that the jet velocity is a governing factor that controls the total energy. Further discussions will be addressed in the following section.

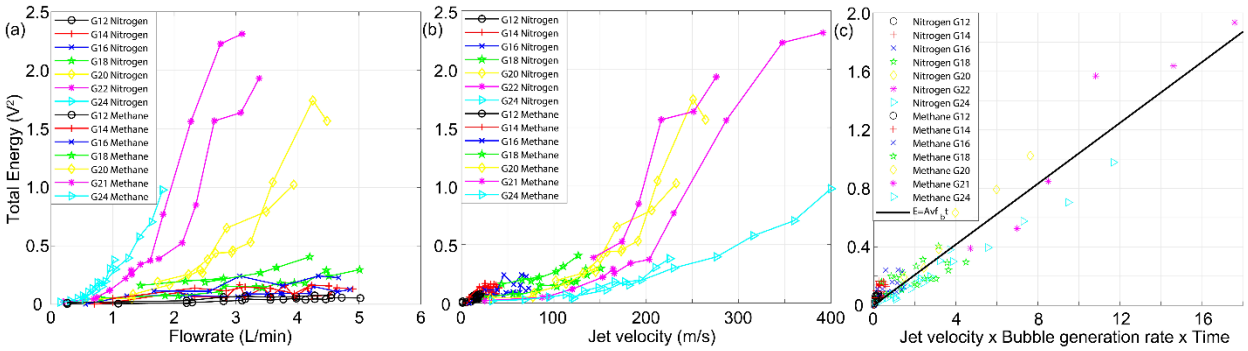

Fig.4 (Color online) (a) Total energy *vs* flow rate, (b) total energy *vs* jet velocity, and (c) total energy *vs* jet velocity× bubble generation rate×time.

4. An empirical relationship and a model

For the constant flow bubble case, an empirical relationship was found among the total energy, flow rate, and needle diameter, expressed by

$$E=BQ^2/D^3t \quad (1)$$

where E denotes the total energy, Q is the flow rate, B is a constant, and t is the time duration of the signal (t=0.3 s, in the study). To better understand this correlation, we assumed that the total energy is a summation of the energy carried by each individual bubble. We further approximated that each single bubble features an identical effective volume. As mentioned before, this effective single bubble volume is proportional to the needle diameter. Using these approximations, we can rewrite the above Eq.(1) in the form expressed as

$$E=B'vf_bt \quad (2)$$

where v is the jet velocity that is proportion to Q/D^2, and f_b is the bubble generation rate that is defined as the flow rate divided by the effective single bubble volume and is proportional to Q/D. As seen in Fig. 4(c), this equation formed a solid line that fitted all experimental data quite well with a coefficient of correlation $|r|^2$ of 0.9. In Eq. (2), the term $B'v$ is interpreted as the energy carried by an effective single bubble and the term f_bt represents the total bubble number. Generally speaking, higher jet velocity can cause higher deformations of bubbles deviating from pure spheres. These distorted bubbles exhibit more oscillation modes than a monopole mode and thus produce greater acoustic energies. On the other hand, as the bubble generation rate f_b increases with the flow rate for a certain needle, more bubbles are created and the chance for bubble coalescence increases. A study [Manasseh *et al*., 2008] demonstrated that the sound created by bubble coalescence has an order of magnitude greater amplitude than the sound created by a bubble pinched off from the needle. These two effects contribute to the total energy for the constant flow case.

5. Conclusions

The acoustic behaviors of bubbles caused by oil leakages were studied in a laboratory under controlled conditions such as flow rate, types of oil leakages, crack sizes, and gases. Specifically, two types of oil leakages were simulated: a few bubble case for oil seepage from sea-floor and the constant flow case for the situation of broken wellheads or pipelines. For a few bubble case, the resonant frequency was proportional to the negative one third of the needle diameter and inversely proportional to the bubble radius, in agreement with the theoretical predications [Minnaert, 1933; Longuet-Higgins *et al*. 1991]. For the constant flow case, the total energy increased with the flow rate and jet velocity. Two equations were obtained to explain the observations. The first equation is an empirical correlation that relates the total energy to oil leakage properties such as flow rate and crack size, and the second is a simple model for bubble-induced sounds in terms of the total energy. These results improve the understanding of bubble-induced sound and are helpful in characterizing oil leakage processes.

Acknowledgments

This research has been funded by Gulf Research Program of the National Academy of Sciences.

References and links

- Deepwater Horizon Study Group, 2011, "Final report on the investigation of the Macondo well blowout", pages 126. https://ccrm.berkeley.edu/pdfs_papers/bea_pdfs/DHSGFinalReport-March2011-tag.pdf

- Leighton, T.G., 1994, “The acoustic bubble”, ISBN 0-12-441920-8 Academic Press Inc., London, NW1 7DX, San Diego, CA 92101
- Leighton, T.G., and A. Walton, 1987, “An experimental study of the sound emitted from gas bubbles in a liquid”, Eur. J. Phys. 8:98-104.
- Longuet-Higgins, M., Kerman, B.R., Lunde, K., 1991. "The release of air bubbles from an underwater nozzle". The Journal of the Acoustical Society of America 89, 2014-2014.
- Lurton, X., 2002, “An introduction to underwater acoustics: principles and applications”, ISBN 3-540-42967-0 Springer-Verlag Berlin Heidelberg New York
- Manasseh, R., Riboux, G., Risso, F., 2008. “Sound generation on bubble coalescence following detachment”. International Journal of Multiphase Flow 34, 938-949.
- Minnaert, M.,1933, "On musical air-bubbles and the sound of running water", Philosophical Magazine, 16 (104): 235–248.
- Reddya, C.M., J. S., Areyb, J.S., Seewalda, S.P., Sylvaa, K.L., Lemkaua, R.K., Nelsona, C.A., Carmichaela, C.P., McIntyrea, J. Fenwickc, G.T., Venturad, B.A.S.V., Mooya, and R., Camillic, 2012, “Composition and fate of gas and oil released to the water column during the Deepwater Horizon oil spill”. Proceedings of the National Academy of Sciences of the United States of America, 109. 20229–20234, doi: 10.1073/pnas.1101242108
- Transportation Research Board Special Report 322, 2016, “Application of Remote Real-Time Monitoring to Offshore Oil and gas operation”, The National Academics Press, ISBN 978-0-309-44242-8 | DOI 10.17226/23499
- Urick, R.J., 1983, “Principles of Underwater Sound”, New York: McGraw-Hill. 3rd ed.